AN EXPERIMENTAL EVALUATION OF THE RESONANT ULTRASONIC SPECTROSCOPY METHOD*

M.C. Remken, C.M. Fortunko, K.W. Hollman, and S. Kim

National Institute of Standards and Technology
Materials Reliability Division
Boulder, CO 80303

INTRODUCTION

For several years we have used Resonant Ultrasonic Spectroscopy (RUS) for routine determination of elastic-stiffness coefficients [1]. RUS has also been used elsewhere as reviewed by Maynard [2] and by Migliori [3]. Therefore, it is important to experimentally establish the uncertainty of the RUS method. Previously, we have compared RUS with pulse-echo superposition and with other resonance methods [4,5]. In this paper, we describe the process we used to determine that the RUS method has a 0.15% uncertainty, which is comparable with our best short-pulse time-of-flight measurement methods.

We used RUS to determine the longitudinal sound velocity in a homogenous, isotropic cylinder of fused silica, which was previously used as a delay line for 25.4 mm diameter transducers. This cylinder is 25.4 mm in diameter and has a length of 25.634 ± 0.002 mm. The density of the cylinder is 2.20162 ± 0.00009 g/cm^3. We established the "true" longitudinal velocity in the same specimen using a number of short-pulse experimental geometries and signal-analysis techniques. The "true" longitudinal velocity was obtained by averaging the results of our best laboratory methods. We report the statistical limits of our estimate of the "true" velocity using a 95% confidence interval [6]. Then we calculated the error between all of the methods and the "true" longitudinal velocity.

Review of Progress in Quantitative Nondestructive Evaluation, Vol. 17
Edited by D.O. Thompson and D.E. Chimenti,, Plenum Press, New York, 1998

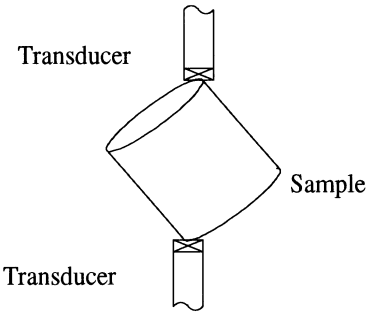

Figure 1. RUS experimental geometry.

RUS METHOD

Figure 1 shows the RUS experimental geometry. We used 1.5 mm diameter piezoceramic element transducers to excite and detect a continuous rf wave produced by a signal generator. The amplitude of the received signal was recorded as a function of the frequency of the excitation signal. Figure 2 shows the RUS spectrum generated by the specimen used in this study. We used an algorithm developed by Heyliger and Ledbetter to convert the resonant frequencies shown in Fig. 2 to the elastic-stiffness coefficients [7].

To determine the longitudinal velocity using the RUS method, we applied the longitudinal modulus (c_l) to the following equation:

$$v_l = \sqrt{\frac{c_l}{\rho}}. \qquad (1)$$

Here, ρ denotes mass density. In our measurement, the apparent c_l is affected by imperfect specimen geometry, air-loading of the specimen and mechanical contact by the transducer supports. Consequently, these effects on the value of c_l could cause a difference between the longitudinal velocity determined using RUS and the "true" longitudinal velocity.

VELOCITY DETERMINATION USING TIME-OF-FLIGHT METHODS

To determine the "true" longitudinal velocity, we used three different experimental geometries and five different signal-analysis techniques. The experimental geometries were all pulse-echo configurations with piezoelectric transducers. Data were acquired using an 8-bit digitizing oscilloscope with a sampling rate of 100 Msamples per second. The signal-analysis techniques were all used to determine the time of flight corresponding to the group-velocity measurement.

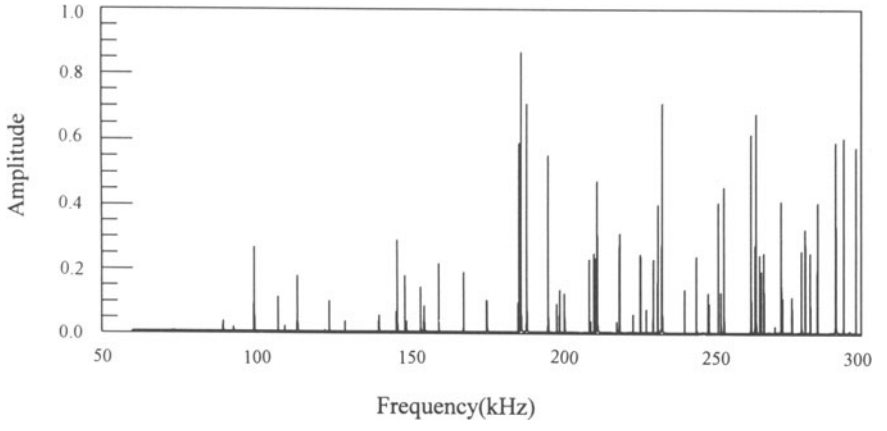

Figure 2. RUS frequency spectrum for fused silica cylinder.

Experimental Geometries

The first experimental geometry used a piezoelectric polymer (PVDF) transducer in a water-immersion tank, as shown in Fig. 3a. The PVDF transducer was broadband (2.3 - 15.1 MHz operating range) with a 10.2 mm diameter, placed at normal incidence nominally 155 mm from the specimen. We excited the transducer using a 5 ns square pulse. The receiver electronics had a bandwidth of 50 MHz.

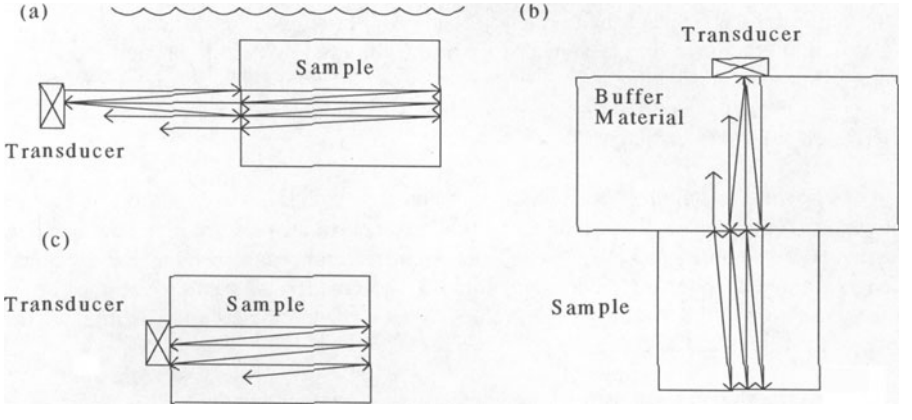

Figure 3. Three experimental time-of-flight geometries: (a) water immersion, (b) buffer rod, (c) direct contact.

The second experimental geometry used a piezoceramic contact transducer coupled to an aluminum buffer rod, as shown in Fig. 3b. The buffer rod was 101.65 mm long with a 50.8 mm diameter. The transducer was broadband (1.5 - 8.5 MHz operating range) with a 12.7 mm diameter. We coupled the transducer and the specimen to the buffer rod with glycerin. We used the same pulser and receiver electronics as in the first geometry.

The third experimental geometry used a direct-contact method, as shown in Fig. 3c, with two different kinds of transducers. The first was the same piezoceramic transducer used in the second experimental geometry. The second kind of transducer was a group of six unbacked quartz transducers. The center frequencies of these transducers were 5, 7, 10, 12, 15 and 17 MHz; the diameters were 10.8, 8.0, 10.4, 8.0, 4.4 and 3.7 mm, respectively. All of the quartz transducers were coaxially plated. We used the same excitation and receiver electronics for the piezoceramic transducer as in the first geometry. We excited the quartz transducers using a tone-burst containing 3-5 cycles. The received signals were high-pass filtered with a cutoff of 4 MHz.

Signal-Analysis Techniques

The first technique we used was pulse-echo superposition [8]. In this method, we visually superimposed the first rise of two separate echoes. We calculated the velocity from the time delay required to satisfy this condition and from the specimen length. We calculated a weighted average of these velocity values, in which the weights were derived from the precision of each velocity calculation.

For the quartz transducers, we used a narrowband pulse-echo overlap method as described by Papadakis [8], instead of the pulse-echo superposition. This method was compatible with the narrowband excitation characteristics of the quartz transducers. The advantage of this method was that the diffraction corrections could be readily applied.

The second technique was an amplitude-spectrum π-point technique, using both broadband and narrowband signals [8,9]. Our implementation of this technique included a correction for the shape of the frequency band [10]. First, we used a linear interpolation scheme to find each resonance of the amplitude spectrum of multiple echoes. Then, we used a linear regression on the π-point resonances as a function of frequency. From the slope of the regression line, we calculated the transit time and determined the group velocity.

The third technique was a phase-spectrum slope technique [11]. First, we "unwrapped" the phase spectrum of each individual echo after performing a windowed discrete Fourier transform. Then, we calculated the difference between the phase of each echo to remove (through deconvolution) common system effects. Next, we applied a linear regression to the resulting phase values. We calculated the group velocity from the slope of the regression line.

The fourth technique was a computed cross-correlation technique [12]. We used the first sinusoidal portion of the first arrival at the transducer as the reference waveform and calculated the cross correlation between that reference and the entire waveform. Transit times were determined using the appropriate maxima of the cross-correlation. The group velocity was calculated from the transit times.

The fifth technique was a time/frequency technique based on the Gabor transform [13]. Here, we calculated a time/frequency image of the signal. This was accomplished by sliding a window along the time axis of the received signal and performing a discrete Fourier transform. Then, we generated an image using the magnitude of each Fourier transform spaced according to the position of the window. We matched the maxima of each echo to calculate the transit time as a function of frequency. Then we determined the velocity as a function of frequency and averaged over frequency to obtain the group velocity. This method is still under development: therefore we did not actually use the results to determine the "true" velocity.

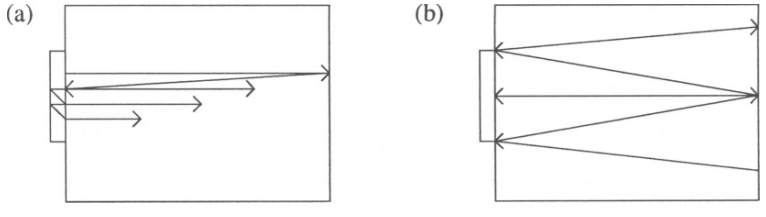

Figure 4. Two physical sources of error for short-pulse time-of-flight methods: (a) finite thickness of transducer, (b) finite diameter of transducer.

All of these signal-analysis techniques determined the velocity from a measurement of the transit time. Consequently, we depend on the following equation:

$$v_l = \frac{L}{\Delta t}. \tag{2}$$

Here L is the length (known to 0.008%), and the transit time Δt is affected by the bandwidth, specimen and transducer geometry, sampling rate and signal-to-noise ratio. Typically, the uncertainty of our transit time is 0.04%, which results in a velocity determination with approximately 0.1% imprecision.

Imprecision and Bias

We considered four sources of bias that may affect the determination of the "true" velocity. First, we explored the effects caused by the face-plate or finite thickness of the transducer. As shown in Fig. 4a, the signal could reverberate within this thickness before being transmitted back into the specimen. This would increase the propagation path length, which would decrease the experimental velocity. Likewise, the transducer had a

finite diameter, which leads to diffraction effects, as shown in Fig. 4b. We calculated a correction for the diffraction effects based on the Lommel diffraction correction integral [14]. The third source of bias was the different temperature of each measurement. Finally, we considered the bias introduced by pulse shape and bandwidth effects.

For the direct-contact geometry, we considered the finite thickness of the quartz transducers. However, the beam spreads by diffraction while propagating through the specimen. Consequently, most of the energy in the wave reflects from a ring outside of the transducer diameter, which leads to velocity values overcorrected by more than 0.5%. We were unable to estimate the effect of the face plate, since its thickness was unknown.

For the water-immersion and buffer-rod geometries, the wave propagates far enough to result in diffraction corrections which are estimated to be less than 0.1%. Also, with the buffer material between the transducer and the specimen, we ignored the finite thickness and face plate of the transducer.

For the direct-contact geometry and the pulse-echo-superposition techniques, we calculated the phase corrections caused by diffraction using the center frequency of each transducer. Following Papadakis [8], we calculated a time correction that is proportional to the phase difference between each echo being considered. For the π-point and phase-slope techniques, we calculated the phase correction caused by diffraction as a function of frequency. Then we calculated a time correction from the slope of this function.

The temperature range of our measurements was from 20.6 to 23.3 °C. Using a handbook value for the coefficient of thermal expansion we estimated that the temperature effect is less than 0.02%. Consequently, we ignored temperature differences.

We have already mentioned a bandshape correction applied to the π-point technique. Through frequency-domain deconvolution, we removed these effects from the phase-slope technique. By using the first arrival of each echo for the superposition techniques, we ignored the pulse-shape effects. Also, since the superposition techniques are strictly in the time domain we did not consider the effects of the bandshape.

EXPERIMENTAL RESULTS

Table 1 shows the velocities used to calculate the "true" longitudinal velocity. The "true" longitudinal velocity in our fused-silica specimen is 5931.2 m/s, with a standard deviation of 3.4 m/s and a 95% confidence interval of 0.11%.[6] Table 2 shows the measured velocities and the residual error from the "true" velocity. We excluded the contact-ceramic measurements from Table 1 because of the large error caused by the face-plate on the transducer. We excluded the contact-quartz results using the frequency spectrum because of the narrowband nature of those echoes. We were unable to use the amplitude-spectrum π-point approach on the buffer rod data because of the extra signals such as side-wall reflections within the specimen. Finally, the phase-spectrum technique on the buffer rod was excluded using an iterative process. We estimated the "true" velocity and calculated residuals from that estimate. Then we removed measurements that were outside the 95% confidence interval and recalculated the "true" velocity.

Using the RUS method, we determined a longitudinal velocity of 5939.8 m/s. The error between this velocity and the "true" velocity is 0.15%, which is slightly greater

Table 1. Velocities (m/s) used to calculate "true" longitudinal velocity of 5931.2 m/s.

	Water Immersion	Direct-Contact Quartz	Buffer Rod
Pulse-Echo Superposition	5930.9	5932.6	5930.4
Amplitude-Spectrum π-point	5927.9	excluded	excluded
Phase-Spectrum slope deconvolution	5924.8	excluded	excluded
Computed X-Correlation	5935.2	5932.7	5933.8

Table 2. Measured velocities and the residual error from the "true" velocity.

Experimental Geometry	Signal-Analysis Technique	Velocity (m/s)	Residual (%)
Water Immersion	Pulse-Echo Superposition	5930.9	0.005
	Amplitude-Spectrum π-point	5927.9	0.056
	Phase-Spectrum Slope Deconvolution	5924.8	0.108
	Computed Cross-Correlation	5935.2	0.067
	Time/Frequency	5929.2	0.034
Buffer Rod	Pulse-Echo Superposition	5930.4	0.013
	Phase-Spectrum Slope Deconvolution	5922.1	0.153
	Computed Cross-Correlation	5933.8	0.044
Contact Quartz	Pulse-Echo Overlap	5932.6	0.024
	Amplitude-Spectrum π-point	5914.3	0.285
	Phase-Spectrum Slope Deconvolution	5885.2	0.776
	Computed Cross-Correlation	5932.7	0.025
Contact Ceramic	Pulse-Echo Superposition	5842.1	1.502
	Amplitude-Spectrum π-point	5879.9	0.865
	Phase-Spectrum Slope Deconvolution	5920.4	0.182
	Computed Cross-Correlation	5885.3	0.774
RUS	Model Calculation	5939.8	0.145

than our 95% confidence interval. Our primary hypothesis for this difference was that the actual fused silica specimen had slightly beveled edges.

SUMMARY

Although the RUS method has an error of 0.15%, it has an uncertainty comparable to our best short-pulse laboratory methods. We can observe this by comparing this error to the errors shown in Table 2. Consequently, we can accurately determine all elastic constants with one measurement on one specimen. This confirms our routine use of RUS for the determination of elastic-stiffness coefficients. We plan to conduct more experimental measurements on cubes and rods of the same material. Another method we will use to experimentally evaluate the RUS method uses a Marx Compound Resonator to measure the elastic constants [4].

ACKNOWLEDGEMENTS

The authors thank Natalia Sizova for her work in acquiring and organizing the early experimental data used in this study.

REFERENCES

1. P. Heyliger, H. Ledbetter and M. Austin, ASTM STP 1045, 100 (1990).
2. J. Maynard, Physics Today 49, 26 (1996)
3. A. Migliori and J.L. Sarrao, *Resonant Ultrasound Spectroscopy* (Wiley-Interscience, New York, 1997)
4. H. Ledbetter, S. Kim, C.M. Fortunko and P. Heyliger, Int. J. Thermophysics 17, 263 (1996)
5. H. Ledbetter, C.M. Fortunko and P. Heyliger, J. Appl. Phys. 78, 1542 (1995)
6. B.N. Taylor and C.E. Kuyatt, NIST Technical Note 1297 (1994).
7. P. Heyliger, A. Jilani, H. Ledbetter, R.G. Leisure and C.-L. Wang, J. Acoust. Soc. Am. 94, 1482 (1993).
8. E.P. Papadakis, *Physical Acoustics, Principles and Methods*, Vol. XII eds. W.P. Mason and R.N. Thurston (Academic Press, New York, 1976), Chap. 5.
9. T. Pialucha, C.C.H. Guyott and P. Cawley, Ultrasonics 27, 270 (1989).
10. W.A. Simpson Jr, J. Acoust. Soc. Am. 56, 1776 (1974).
11. W. Sachse and Y.-H. Pao, J. Appl. Phys. 49, 4320 (1978).
12. J.-D. Aussel and J.-P. Monchalin, Ultrasonics 27, 189 (1989).
13. D. Gabor, J. IEEE 93, 429 (1946).
14. P.H. Rogers and A.L. Van Buren, J. Acoust. Soc. Am. 55, 724 (1974).